

BICEP Array cryostat and mount design

Michael Crumrine^a, P. A. R. Ade^b, Z. Ahmed^c, R. W. Aikin^d, K. D. Alexander^e, D. Barkats^e, S. J. Benton^f, C. A. Bischoff^g, J. J. Bock^{d,h}, R. Bowens-Rubin^e, J. A. Brevik^d, I. Buder^e, E. Bullockⁱ, V. Buza^{e,j}, J. Connors^e, J. Cornelison^e, B. P. Crill^h, M. Dierickx^e, L. Duband^k, C. Dvorkin^j, J. P. Filippini^{l,m}, S. Fliescher^a, J. Graysonⁿ, G. Hall^a, M. Halpern^o, S. Harrison^e, S. R. Hildebrandt^{d,h}, G. C. Hilton^p, H. Hui^d, K. D. Irwin^{c,n,p}, J. H. Kangⁿ, K. S. Karkare^{e,q}, E. Karpelⁿ, J. P. Kaufman^r, B. G. Keating^r, S. Kefeli^d, S. A. Kernasovskiyⁿ, J. M. Kovac^{e,j}, C. L. Kuo^{c,n}, K. Lau^a, N. A. Larsen^q, E. M. Leitch^q, M. Lueker^d, K. G. Megerian^h, L. Moncelsi^d, T. Namikawa^s, H. T. Nguyen^h, R. O'Brient^{d,h}, R. W. Ogburn IV^{c,n}, S. Palladino^g, C. Pryke^{a,i}, B. Racine^e, S. Richter^e, R. Schwarz^a, A. Schillaci^d, C. D. Sheehy^{q,u}, A. Soliman^d, T. St. Germaine^e, Z. K. Staniszewski^{d,h}, B. Steinbach^d, R. V. Sudiwala^b, G. P. Teply^{d,r}, K. L. Thompson^{c,n}, J. E. Tolanⁿ, C. Tucker^b, A. D. Turner^h, C. Umiltà^g, A. G. Vieregg^{q,v}, A. Wandui^d, A. C. Weber^h, D. V. Wiebe^o, J. Willmert^a, C. L. Wong^{e,j}, W. L. K. Wu^{n,q}, E. Yangⁿ, K. W. Yoon^{c,n}, and C. Zhang^d

^aSchool of Physics and Astronomy, University of Minnesota, Minneapolis, MN 55455, USA

^bSchool of Physics and Astronomy, Cardiff University, Cardiff, CF24 3AA, United Kingdom

^cKavli Institute for Particle Astrophysics and Cosmology, SLAC National Accelerator Laboratory, Menlo Park, CA 94025, USA

^dDepartment of Physics, California Institute of Technology, Pasadena, CA 91125, USA

^eHarvard-Smithsonian Center for Astrophysics, Cambridge, MA 02138, USA

^fDepartment of Physics, University of Toronto, Toronto, Ontario, M5S 1A7, Canada

^gDepartment of Physics, University of Cincinnati, Cincinnati, OH 45221, USA

^hJet Propulsion Laboratory, Pasadena, CA 91109, USA

ⁱMinnesota Institute for Astrophysics, University of Minnesota, Minneapolis, MN 55455, USA

^jDepartment of Physics, Harvard University, Cambridge, MA 02138, USA

^kService des Basses Températures, Commissariat à l'Energie Atomique, 38054 Grenoble, France

^lDepartment of Physics, University of Illinois at Urbana-Champaign, Urbana, IL 61801, USA

^mDepartment of Astronomy, University of Illinois at Urbana-Champaign, Urbana, IL 61801, USA

ⁿDepartment of Physics, Stanford University, Stanford, CA 94305, USA

^oDepartment of Physics and Astronomy, University of British Columbia, Vancouver, British Columbia, V6T 1Z1, Canada

^pNational Institute of Standards and Technology, Boulder, CO 80305, USA

^qKavli Institute for Cosmological Physics, University of Chicago, Chicago, IL 60637, USA

^rDepartment of Physics, University of California at San Diego, La Jolla, CA 92093, USA

^sLeung Center for Cosmology and Particle Astrophysics, National Taiwan University, Taipei 10617, Taiwan

^tCanadian Institute for Advanced Research, Toronto, Ontario, M5G 1Z8, Canada

^uPhysics Department, Brookhaven National Laboratory, Upton, NY 11973

^vDepartment of Physics, Enrico Fermi Institute, University of Chicago, Chicago, IL 60637

Further author information: (Send correspondence to M. Crumrine)

M. Crumrine: E-mail: crumrine@umn.edu

ABSTRACT

BICEP Array is a cosmic microwave background (CMB) polarization experiment that will begin observing at the South Pole in early 2019. This experiment replaces the five BICEP2 style receivers that compose the *Keck Array* with four larger BICEP3 style receivers observing at six frequencies from 30 to 270GHz. The 95GHz and 150GHz receivers will continue to push the already deep BICEP/*Keck* CMB maps while the 30/40GHz and 220/270GHz receivers will constrain the synchrotron and galactic dust foregrounds respectively. Here we report on the design and performance of the BICEP Array instruments focusing on the mount and cryostat systems.

Keywords: Inflation, Gravitational Waves, Cosmology, BICEP, Keck Array, Polarization, BICEP Array

1. INTRODUCTION

Precision measurements of the cosmic microwave background have significantly increased our understanding of the early universe. Beginning with the discovery of the CMB—providing the first evidence for a Big Bang origin to the universe^{1,2}—experimental cosmology has become an extremely active subfield of physics. Subsequently the development of the Λ CDM cosmological model has seen tremendous success in its ability to accurately and self-consistently explain and predict experimental data. The Λ CDM model is, however, still incomplete and fails to explain the homogeneity and isotropy of our observable universe. These issues can be resolved by an extension to the model in which the universe undergoes a period of exponential expansion known as inflation just after the initial Big Bang.³ Various models of inflation exist, many of which predict that such an event would have generated a gravitational wave background. Interaction between these inflationary gravitational waves (IGWs) and the CMB would have produced a characteristic curl-like polarization signal colloquially referred to as “B-modes”. Measurement of this signal is generally characterized by the tensor to scalar ratio r , which can also be used as a measure of the energy scale of inflation as well as to differentiate inflationary models.

Detection of the inflationary B-mode signal is complicated by the presence of other B-mode signals. At small angular scales, lensing of divergence-like CMB polarization can convert so called “E-modes” into B-modes through small angular remappings. Other sources of B-mode signal exist in our own galaxy. Polarized emission from galactic dust and galactic synchrotron radiation are the two dominant foregrounds in our own galaxy, each characterized by independent frequency and angular scale relations. Detection of any primordial B-mode signal requires observations at multiple frequencies to enable its separation from these foregrounds.

The BICEP/*Keck* experiments are a staged series of microwave telescopes that observe the CMB from the geographic South Pole and target degree-scale B-mode polarization. Each successive generation of telescope builds upon the experience gained with the previous while simultaneously increasing sensitivity. A graphical progression from BICEP2 to BICEP Array is shown below in Fig. 1. Foreground signals exhibit strong frequency dependence which allows these components to be isolated from the IGW signal by observing the microwave sky across a range of frequencies. *Keck Array* consists of five BICEP2 style receivers with observations spread across four frequency bands (95, 150, 220, and 270 GHz). The combination of BICEP2 and *Keck Array* data has produced the strictest constraint on this signal to date of $r < 0.07$.⁴ BICEP Array builds on the success of the *Keck Array* by deploying four BICEP3 style receivers and expanding observations into two additional frequency bands at 30 and 40 GHz. Extrapolating from achieved performance, BICEP Array is projected to reach $\sigma(r) < 0.004$, either detecting the IGW signal or improving the constraint to $r < 0.008$.

2. CRYOSTAT DESIGN

BICEP Array continues the successful design philosophy of the previous BICEP/*Keck* receivers. An 80" tall vacuum shell contains two nested stages with nominal operating temperatures of 50K and 4K which accommodate optical elements and shield the sub-Kelvin receiver. A cross section of the cryostat is shown in Fig. 2. The top section of the vacuum jacket houses the vacuum window and a stack of Zote foam filters which reduce infrared loading onto the colder stages. The use of low-conductivity structural supports keeps the interior stages sufficiently supported while conducting only a small amount of heat from the room temperature vacuum vessel. These supports are described in more detail in Sec. 3. The intermediate 50K stage serves as a radiation shield for the interior 4K stage. The lower $\sim 70\%$ of the 50K stage is wrapped with a 0.04"-thick magnetic shield composed of Amuneal

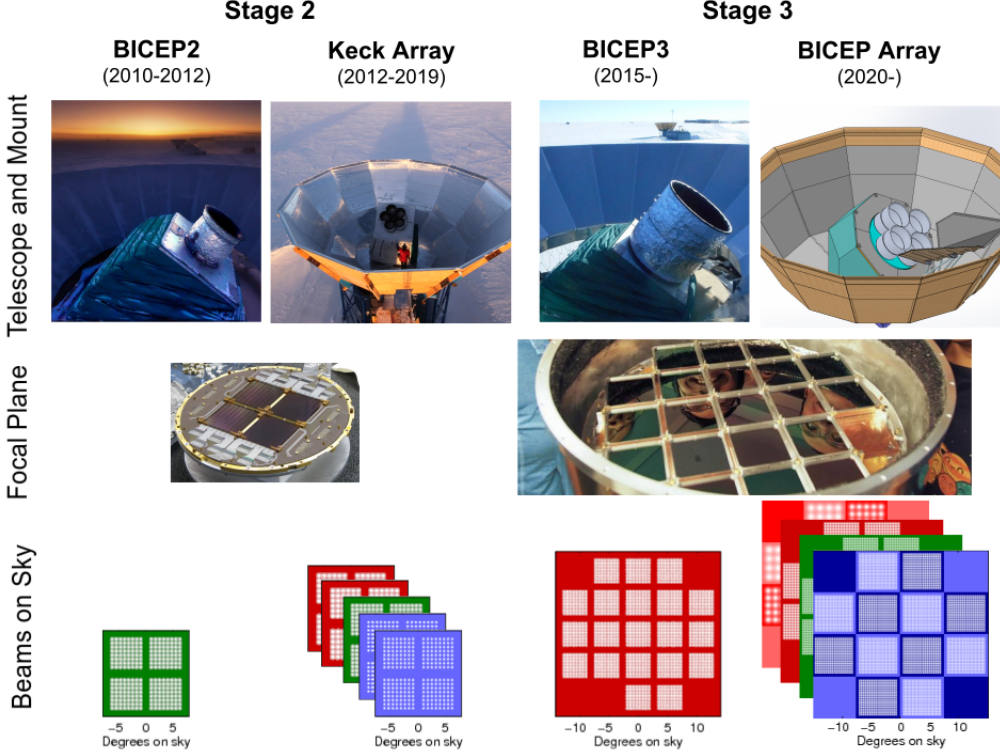


Figure 1. A graphical representation of the BICEP/Keck experiments from BICEP2 through BICEP Array. The middle and bottom rows show the increased focal plane size and density of the BICEP3 style receivers as compared to the BICEP2 style. Different frequencies are represented in the bottom row by individual colors with the lowest frequency (30 GHz) visible in light red and the highest (270 GHz) visible in dark blue.

A4K. The top of this stage additionally accommodates an alumina filter to further reduce infrared loading onto the sub-Kelvin receiver. The 4K stage serves as a second radiation shield while also providing mounting interfaces for two alumina lenses and optical baffling.

The cryostat design enables ease of access to the focal plane assembly without disturbing the majority of thermal joints or the back-end cabling. The cryostat disassembles by lifting off shells successively from the outside in, leaving a stand-alone base behind which contains the sub-Kelvin focal plane assembly, readout electronics, and the cooling system as shown in Fig. 3. In this state, the focal plane and detector modules may be freely accessed for maintenance. Access to the underside of the focal plane and the readout electronics is provided by hatches on the bottom side of the vacuum shell and 50K bases. This scheme significantly reduces the time required for disassembly when accessing the focal plane and re-assembly afterwards by allowing critical thermal junctions and difficult part matings to remain undisrupted.

3. THERMAL ARCHITECTURE

The 50K and 4K radiation shields are cooled by the first and second stages of a Cryomech PT415-RM Pulse Tube cooler respectively. This cryocooler is capable of maintaining a first stage temperature of $< 45\text{K}$ under a 40W load and a second stage temperature of $< 4\text{K}$ under a 1.5W load. The cooler of these two stages is required to maintain a sufficiently cold temperature to allow the operation of a three-stage helium sorption fridge which cools the sub-Kelvin focal plane assembly. The interior stages must therefore be well insulated in order to stay within the thermal budget.

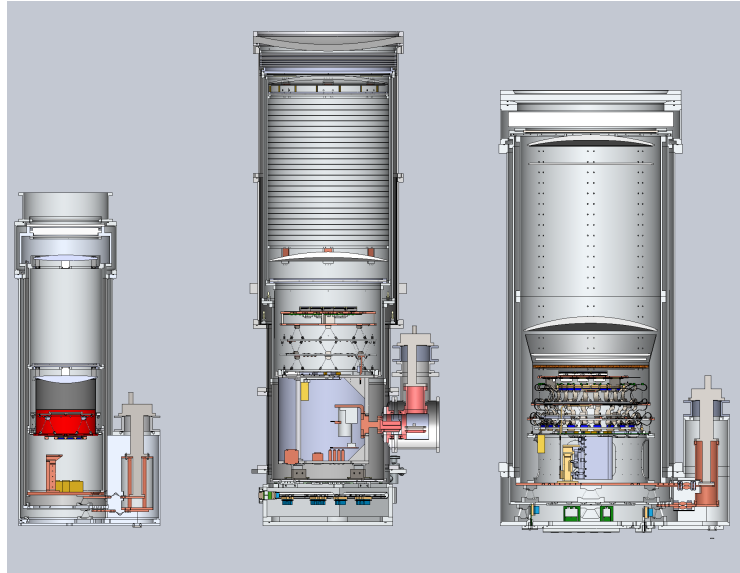


Figure 2. A CAD cross section of a single *Keck Array* receiver (left), the BICEP3 receiver (middle), and a single BICEP Array receiver (right). The BICEP Array receivers have double the clear aperture and significantly increased focal plane density as compared to the *Keck Array* receivers. BICEP Array also increases the width of the cryostat compared to BICEP3 in order to include more optical baffling at the lowest frequencies.

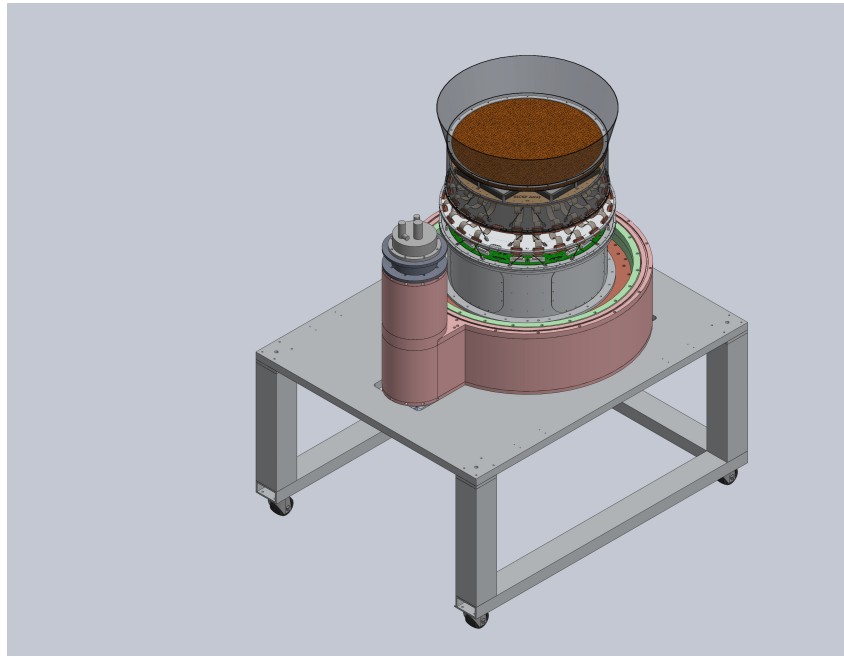


Figure 3. A partially disassembled BICEP Array cryostat. In this view the long upper sections of the vacuum jacket, 50K, and 4K stages have been removed leaving behind the base assembly that contains the pulse tube cooler, focal plane assembly, and the readout electronics. Elevating this base structure onto a lab stand allows hatches on the bottom side of the cryostat to be opened for access to the backend without disturbing the focal plane or any thermal joints.

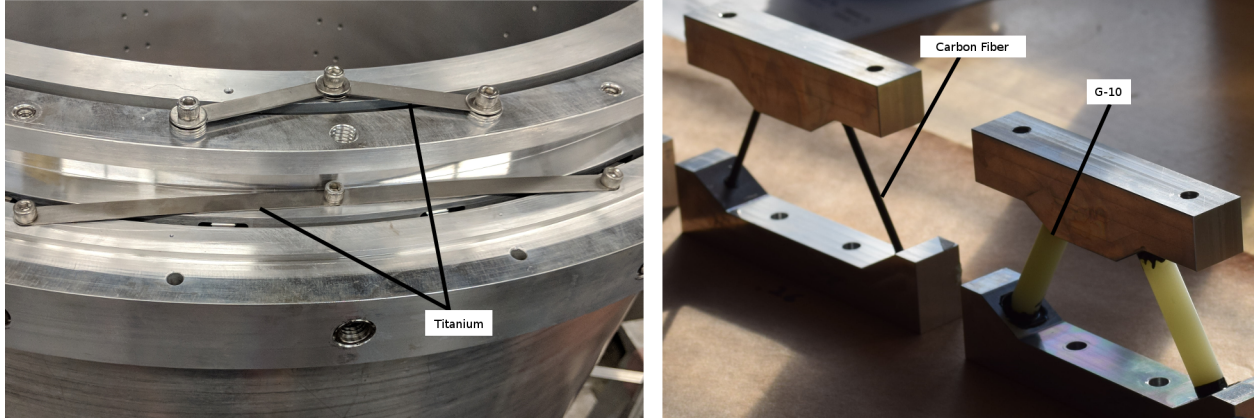


Figure 4. **Left:** The top end titanium supports. These thin strips are flexible along the axial direction of the cryostat while rigid enough to maintain concentricity of the stages. **Right:** Example carbon fiber (left) and G10 (right) supports. These supports sit at the back end of the cryostat and span the gap between the vacuum jacket to 50K stage (G10) and between the 50K and 4K stage (carbon fiber). Each rod is held in place with Stycast epoxy.

The radiation absorbed by the interior stages is reduced by the use of multi-layer insulation (MLI) wrapped around the outside of the 50K and 4K stages. These MLI blankets are composed of many aluminized Mylar layers separated by polyester spacer layers. Where there is insufficient room for uncompressed insulation, high emissivity aluminum tape is used on parallel faces to decrease the radiation absorbed by the lower temperature surface. A low thermal conductivity support system keeps the three stages thermally insulated from each other and provides structural support. The front end of each shell is constrained by thin Ti-Al-4V straps which allow flexing along the axial direction of the cryostat to absorb differential thermal contraction. At the back end, the 50K and 4K stages are each supported by six trusses. Each truss has two high tensile strength / thermal conductivity rods bonded to aluminum blocks with Stycast epoxy. We use G10-FR4 for the back-end supports between the vacuum shell and the 50K radiation shield but switch to carbon fiber between the 50K and 4K shells due to the latter's lower thermal conductivity at low temperatures. Figure 4 shows fabricated examples of the front and back-end supports.

In addition to providing radiation shielding and mount points for low temperature optics, the 50K and 4K stages provide natural heat sinks for the cryocables that connect the sub-Kelvin electronics to the exterior room-temperature data acquisition system. By sinking the cryocables to the 50K stage, the conductive loading beyond the 50K stage is significantly reduced. Likewise, the heatsinks on the 4K stage further reduce the conductive loading into the sub-Kelvin assembly.

4. COPPER BRAID HEAT STRAPS

The heat straps connecting the pulse tube cooler to the 50K and 4K stages of the cryostat needs to have large thermal conductance but also be fairly flexible to suppress vibrations transmitted to the focal plane. BICEP Array uses custom made oxygen-free high thermal conductivity (OFHC) copper assemblies each composed of multiple straps. As shown in Fig. 5 each heat strap consists of two end blocks connected by a series of multi-layered braided wire straps. The braided straps comprise seven layers of OFHC braid pressure fused into a small diameter OFHC pipe section on either end. The pressure fusing is performed by a hydraulic press under a load of 20 tons with lateral constraint provided by a steel die. We have been able to achieve thermal conductance of $G = 600 \frac{\text{mW}}{\text{K}}$ @4K per strap in laboratory tests.

The heat straps in the BICEP Array cryostat combine a number of these straps to achieve high total thermal conductance. Two layers of braided straps are sandwiched around an OFHC plate on both ends. These plates provide mounting interfaces to the rest of the cryostat and the pulse tube cooler. Stainless steel plates on the top and bottom sides of this interface allow the use of 1/4" stainless steel bolts to create a high pressure joint and reduce thermal contact resistance. Figure 5 shows a fully assembled heat strap assembly that interfaces between the 4K radiation shield and the second stage of the pulse tube.



Figure 5. **Left:** A completed heat strap composed of 6 braided straps. A thin steel plate distributes the force of the bolts and nuts across the surface of the braid ends. **Right:** A single 7-layer braided strap. This strap is created by inserting layers of OFHC braid into a short OFHC tube and compressing under 20 tons of pressure in a hydraulic press.

5. MOUNT AND OPERATIONS

The larger size of the BICEP Array as compared to the *Keck Array* it replaces requires a larger motorized platform for operation. Designed by Eric Chauvin, the new BICEP Array mount uses the same three axis design as the previous BICEP/*Keck* experiments which augments the azimuth and elevation axes with rotation about the boresight of the array. A cross section of the new mount assembly is shown below in Fig. 6. As with previous BICEP/*Keck* experiments, the cryostats are enclosed within an accordion-like environmental shield which co-rotates in azimuth and flexes as the mount tips in elevation. A separate forward plate provides a mounting interface for four optical baffles—one per receiver—and co-rotates with the receivers about the array boresight.

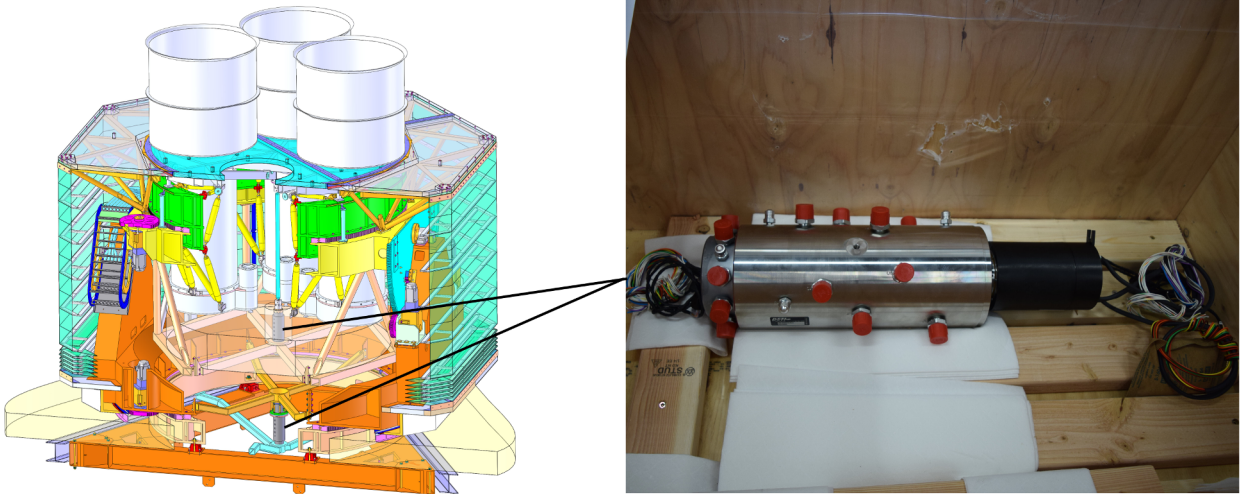


Figure 6. **Right:** A CAD rendering of the new BICEP Arraymount and cryostats. The surrounding accordion-like environmental shield is shown in teal while the two rotary unions are depicted in gray and can be seen along the central axis of the mount. The large cylinders on the top side of the mount assembly are the co-moving absorptive optical baffles that reduce sidelobe response. A fixed ground shield (not shown) surrounds this mount assembly and reduces pickup from ground-fixed sources. Black lines indicate the two rotary unions. **Left:** One of the rotary unions from DSTI. Red caps denote the locations of helium lines. The electrical and data connections can be seen exiting either end of the union.

The BICEP Array mount includes two separate rotary unions which allow continuous rotation about the azimuth axis and array boresight without the need for a cable wrap. These rotary unions were designed at DSTI, and each contain 10 helium channels. Eight of these connect the pulse tubes and their compressors, while two channels serve as pressure guards. An additional nitrogen channel provides a pressurized environment on front end of the cryostats which shields the receivers' vacuum windows from the Antarctic winter. Slip rings at both ends of the union additionally provide data and power connections to electronics across separately rotating stages of the mount. These rotary unions allow the helium compressors—required to operate the pulse tube coolers—to sit well below the mount structure in the stationary tower. Helium lines route upwards into the lower (ground fixed) half of the first rotary union and then out through the upper half which rotates in azimuth along with the receivers. The hoses from the upper half are then routed through a short cable chain that provides flexure when rotating in elevation. The second rotary union is then similarly connected across the elevation and boresight axes.

BICEP Array will consist of four receivers observing in 6 frequency bands. Two receivers will continue to observe in the 95 and 150 GHz bands where the BICEP/*Keck* maps are deepest and where combined foreground signal is at a minimum. These will be augmented by two dual-band receivers at 30/40 GHz and 220/270 GHz. The 30/40 GHz receiver will extend the observations into two new bands at which the synchrotron foreground is expected to dominate. The *Keck Array* is already observing in the 220 and 270 GHz bands. However with significantly increased throughput and a detector count of over 9 times the entire *Keck Array*, the dual band 220/270 GHz BICEP Array receiver will rapidly eclipse current sensitivity. In only a few days of observation, this receiver will surpass the dust sensitivity of the *Planck* 353 GHz data in the BICEP/*Keck* field. With the increased sensitivity at 95 and 150 GHz, these two additional receivers will be required to push constraints on polarized emission from galactic synchrotron and dust further than the currently available data.

The 30/40 GHz receiver will extend the observations into two new bands at which the synchrotron foreground is expected to dominate. The *Keck Array* is already observing in the 220 and 270 GHz bands. However with significantly increased throughput and a detector count of over 9 times the entire *Keck Array*, the dual band 220/270 GHz BICEP Array receiver will rapidly eclipse current sensitivity. In only a few days of observation, this receiver will surpass the dust sensitivity of the *Planck* 353 GHz data in the BICEP/*Keck* field.

The observing power of BICEP Array will be concentrated on the same $\sim 400 \text{ deg}^2$ ($\sim 600 \text{ deg}^2$ for BICEP3 generation) patch of sky as the existing BICEP/*Keck* data. By directly observing cosmological foregrounds with the new dual band receivers in the patch at which the BICEP/*Keck* data is already the deepest, we will be able to directly constrain these foregrounds in our own patch of sky, significantly reducing the effect of any spatial variation in the foregrounds' spectral energy distribution. Increasing foreground constraints will be complemented by simultaneously increasing sensitivity to r with the single band receivers. Figure 7 shows the sensitivity projections for BICEP Array. All projections are based on achieved sensitivity and as such, build in real world inefficiencies such as detector yield, weather, and other factors which decrease overall sensitivity. By the end of the program, BICEP Array is projected to constrain $r < 0.008$, $\sigma(r) < 0.004$.

REFERENCES

- [1] Penzias, A. A. and Wilson, R. W., "A Measurement of Excess Antenna Temperature at 4080 Mc/s.," *Astrophys. J.* **142**, 419–421 (July 1965).
- [2] Dicke, R. H., Peebles, P. J. E., Roll, P. G., and Wilkinson, D. T., "Cosmic Black-Body Radiation.," *Astrophys. J.* **142**, 414–419 (July 1965).
- [3] Guth, A. H., "Inflationary universe: A possible solution to the horizon and flatness problems," *Phys. Rev. D* **23**, 347–356 (Jan. 1981).
- [4] The BICEP2 and *Keck Array* Collaborations, "BICEP/*Keck* VI: Improved Constraints on Cosmology and Foregrounds from BICEP2 and *Keck Array* Cosmic Microwave Background Data with Inclusion of 95 GHz Band," *Phys. Rev. Lett.* **116**, 031302 (Jan. 2016).
- [5] The BICEP/*Keck* and *Planck* Collaborations, "Joint Analysis of BICEP/*Keck* and *Planck* Data," *Phys. Rev. Lett.* **114**, 101301 (Mar. 2015).

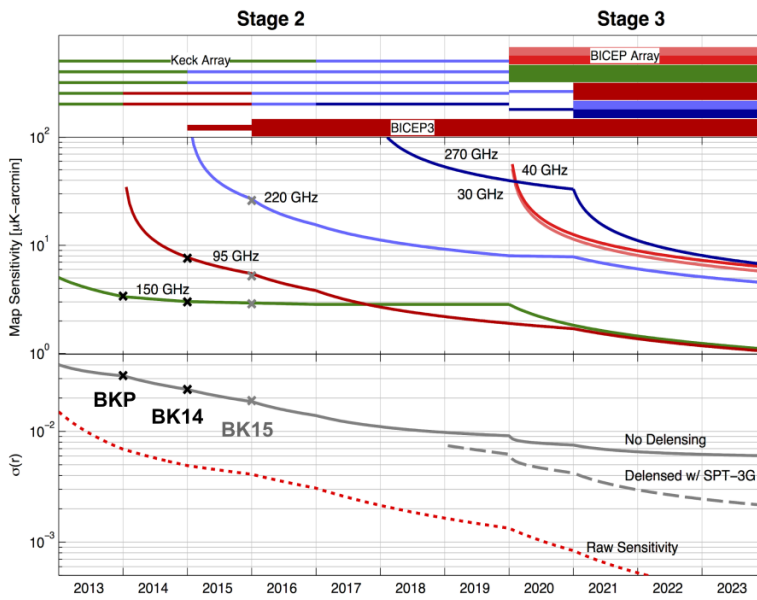


Figure 7. Achieved and projected sensitivity for the current and planned BICEP/Keck program. **Top:** A representation of receiver throughput at different frequencies. **Middle:** Achieved and projected map depth at various frequencies as a function of time. Black X's mark achieved sensitivities in the BKP⁵ and BK14⁴ papers, while gray X's show achieved sensitivity in the upcoming BK15 paper. **Bottom:** Sensitivity to r , marginalizing over the seven parameter foreground model as described in BK14. Raw sensitivity in the absence of foregrounds is also shown.